Accepted Manuscript

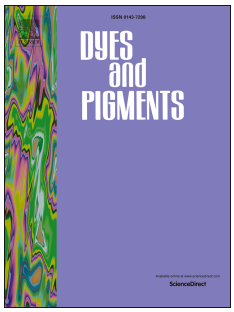

An AIE dye based smartphone and LDA integrated portable, intelligent and rapid detection system as trace water indicator and cyanide detector

Linfeng Chen, Xike Tian, Yong Li, Chao Yang, Liqiang Lu, Zhaoxin Zhou, Yulun Nie

PII: S0143-7208(19)30268-2

DOI: https://doi.org/10.1016/j.dyepig.2019.03.008

Reference: DYPI 7397

To appear in: *Dyes and Pigments*

Received Date: 2 February 2019

Revised Date: 27 February 2019

Accepted Date: 5 March 2019

Please cite this article as: Chen L, Tian X, Li Y, Yang C, Lu L, Zhou Z, Nie Y, An AIE dye based smartphone and LDA integrated portable, intelligent and rapid detection system as trace water indicator and cyanide detector, *Dyes and Pigments* (2019), doi: https://doi.org/10.1016/j.dyepig.2019.03.008.

Graphical Abstract

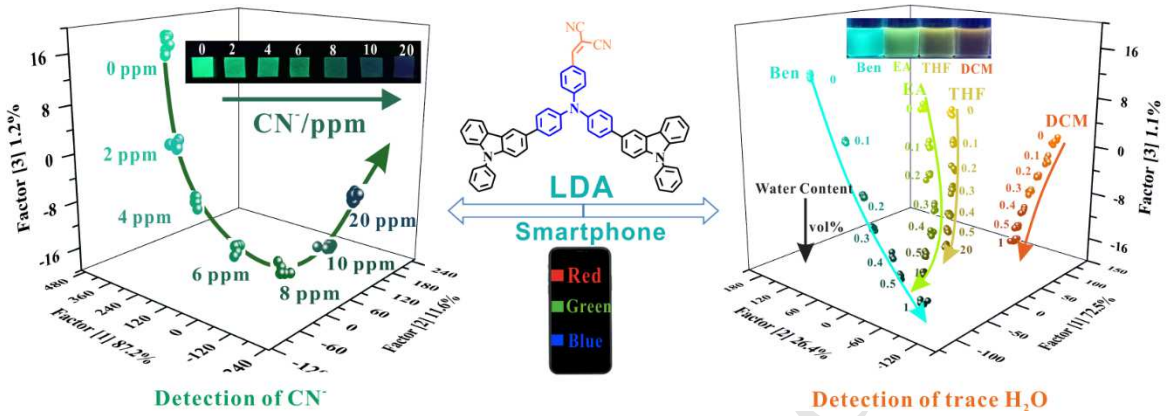

An AIE dye based smartphone and LDA integrated portable, intelligent and rapid detection system as trace water indicator and cyanide detector

Linfeng Chen, Xike Tian*, Yong Li, Chao Yang, Liqiang Lu, Zhaoxin Zhou and Yulun Nie

Faculty of Materials Science and Chemistry, China University of Geosciences, Wuhan 430074, China

Corresponding author: Xike Tian(xktian@cug.edu.cn)

Abstract:

Portable, rapid, accurate and on-site detection of analysis target has always been the goal of continuous efforts in the field of analysis. In this work, a novel intelligent and rapid detection system based on an AIE dye (TPA-DCV) was established for portable and on-site detection of trace water in organic solvents and CN^- in water by integrating the smartphone and linear discriminant analysis (LDA). The TPA-DCV displayed remarkable solvatochromism effect and showed different fluorescence colors to different water contents of different solvents, with the minimum detection limit of 54 ppm. In addition, TPA-DCV also exhibited specific response to CN^-, and showed significant fluorescence changes to different amounts of CN^-. With the assist of this detection system, these different fluorescence color signals could be accurately classified in canonical score plot. What's more, the classification and distribution of fluorescence color in canonical score plot showed regular change with the target concentration, which could be used to quantify the trace water and CN^-. The rationality and practicability of this detection system were preliminary verified by a large number of real sample analyses. This detection system greatly simplifies the analysis process, which is in the proof of intelligent and rapid detection just using a simple color analysis without any instrument test, which may be a big step forward.

Keywords: Cyanide detection; Water detection; Smartphone; Linear discriminant analysis

1. Introduction

Cyanide (CN^-) is considered as the most toxic anion in environment. Even small doses of CN^- are fatal to mammals due to its tendency to bind with iron species in cytochrome c oxidase, which destructs electron transport and lead to hypoxia [1-4]. However, cyanide is also an important industrial raw material, widely used in electroplating, paint, dye, rubber and other industries, posing continuous contamination problems. Therefore, accurate detection of CN^- levels in groundwater is of great significant. On the other hand, the accurate analysis of trace water in organic solvents is also of great importance for many industrial applications. especially in organic synthesis, pharmaceutical manufacturing and oil industry [5, 6]. Although many techniques have been reported for monitoring trace water or CN^-, effective rapid detection methods are rarely reported [7-13]. Many researchers are committed to developing paper sensors for visual on-site monitoring because none of instrument testing are required, which greatly simplifies the detection process [14-16]. However, the determination of concentration just by observing the color of the test paper is inaccurate [17-21]. How to accurately establish the relationship between the target concentration and the color signal is a meaningful but neglected work.

Mobile phones are indispensable device for everyone, and the equipment of smart chip and high-definition (HD) camera endow smartphone with high-speed computing and camera capabilities. With the aid of HD camera and color recognition APP, the detail optical information from the color of samples, such as color properties: hue, brightness and saturation, or color parameters: red, green and blue, can be easily obtained.[22] We found that a few of reports have realized the accurate visual inspection by establishing a linear relationship between color parameters and target concentration[23]. However, it should be pointed out that these works were all using single color channel changes (red, green or blue) to establish the relationship with target. As we known, the parameters for each color are unique and the change of color will cause the parameter changes of three color channels. Even if only the lightness of the color changes, the red, green or blue parameters will change drastically. Therefore, quantitative analysis based on single-channel color parameter changes is still not accurate enough. Establishing an accurate relationship between color and target concentration remains a serious challenge. Linear discriminant analysis (LDA), owning to its powerful recognition and identification capabilities [24-28], has been widely used in artificial intelligence and neural networks, which is an integral part of pattern recognition [29-31]. If we use LDA to analyze the color parameters of red, green and blue channels, the similar colors should be accurately classified and the different colors should be distinguished. What's more, according to the classification of existing standard samples, the concentration unknown samples could be intelligently identified, just like fingerprint or facial

recognition.

Inspired by this, we first established an intelligent and rapid detection system based on an AIE dye (TPA-DCV) by integrating smartphone and LDA for portable and rapid trace detection of water and CN^-. The AIE dye displayed remarkable solvatochromism effect and showed different fluorescence colors to different water contents of different organic solvents. The detection limit for water was as low as 0.0048% (54 ppm), which was comparable to the classical Karl-Fischer method. In addition, TPA-DCV also exhibited specific response to CN^- and showed significant fluorescence changes to different amounts of CN^-. The detection limit for CN^- was calculated to be 0.16 μM which was much lower than the drinking water standard. This different fluorescence colors changes for water or CN^- could be accurately classified in canonical score plot using the smartphone and LDA integrated detection system. What's more, the classification and distribution of fluorescence color in canonical score plot showed regular changes with target concentration, which could be used to quantify the target. The rationality and practicability of this detection system were preliminary verified by a large number of real sample analyses. This detection system does not require any instrument testing and the target concentration can be detected just by color analysis, which greatly simplifies the testing process and provides new ideas for the development of portable and rapid detection technology.

2. Experimental section

2.1 Reagents and instruments

The organic reagents 3-bromo-*N*-phenylcarbazole, *n*-butyllithium, trimethyl borate, $Pd[P(Ph)_3]_4$, malonitrile, 4-(N,N-diphenylamino) benzaldehyde were purchased from Aladdin and used as received. Organic solvents are strictly dewatered before use. The cyanide anion used in whole experiments is tetrabutylammonium salt, the others are the corresponding sodium or potassium salt.

The obtained products in this work were characterized by ^{1}H-NMR (Bruker Avance 400 MHz NMR spectrometer), ^{13}C-NMR and HRMS (GCT premier CAB048 mass spectrometer). Fluorescence spectra of TPA-DCV were collected using HITACHI F-7000 fluorescence spectrometer. The absorption signals of TPA-DCV were obtained from a Perkin Elmer Lambda 35 spectrophotometer. Particle size change before and after reaction of TPA-DCV with CN^- was monitored by an ALV-5000 dynamic laser light scattering (DLS).

2.2 Synthesis of (3-carbazol-9-ylphenyl)boronic acid (1)

3.1 mmol (1.0 g) of 3-bromo-*N*-phenylcarbazole was added in a 100 mL three-neck flask. In a nitrogen atmosphere, 15 mL of THF was injected into the three-neck flask to dissolve the raw material and then cooled in liquid nitrogen. After the solution was cooled to -78°C, 2 mL (3.2 mmol) of *n*-butyllithium was dropped into the mixture by syringe and then keep stirring for 1 h. Then, 380 μL (3.4 mmol) of trimethyl borate was introduced into the mixture and stirred at room temperature for 12 h. After reaction, 20 mL of HCl (1 M) was poured into the mixtures and stirred vigorously, followed by the addition of 50 mL of ethyl acetate to extract product. 100 mL of saturated sodium bicarbonate was used to wash the collected organic layer, and then 10 g of magnesium sulfate was used to dry the washed organic layer. Finally, the white product was obtained by reduced pressure and further dried in a vacuum oven (78.6% yield). ^{1}H NMR (400 MHz, $CDCl_3$, δ (TMS, ppm): 7.67 (t, *J* = 8.8 Hz, 5H), 7.56 (m, *J* = 10.8 Hz, 3H), 7.45 (d, *J* = 4.2 Hz, 2H), 7.41 (m, *J* = 7.4 Hz, 2H), 2.15 (s, 2H). ^{13}C NMR (100 MHz, $CDCl_3$), δ (TMS, ppm): 143.84, 141.22, 137.47, 133.37, 129.93, 128.71, 127.72, 127.20, 127.12, 126.10, 123.65, 123.31, 120.62, 120.47, 109.95, 109.37.

2.3 Synthesis of 4-di(4-iodophenyl)aminobenzaldehyde (2)

2.4 g (14.6 mmol) of potassium iodide and 2 g of (7.3 mmol) 4-Diphenylaminobenzaldehyde was first introduced into 100 mL of acetic acid and 10 mL distilled water to dissolve the raw materials. The mixtures were allowed to react in an oil bath at 80 °C for 0.5 h. Then, 2.4 g (11.0 mmol) of potassium iodate was added and kept reacting for another 4 hours. After the reaction,

200 mL of distilled water was introduced into the cooled mixture to precipitate crude product. The brown crude products were washed three times with saturated $Na_2S_2O_3$ solution to give 3.2 g of yellow solid (yield 84%). ^{1}H NMR (400 MHz, $CDCl_3$), δ (TMS, ppm): 9.84 (s, 1H), 7.72 (d, J = 8.1 Hz, 2H), 7.64 (d, J = 7.8 Hz, 4H), 7.06 (d, J = 7.8 Hz, 2H), 6.90 (d, J = 7.6 Hz, 4H). ^{13}C NMR (100 MHz, $CDCl_3$), δ (TMS, ppm): 90.17, 120.53, 128.44, 131.79, 139.18, 145.74, 152.20, 191.34. HRMS (m/z): $[M+H]^+$ calcd. for $C_{19}H_{13}I_2NO$, 525.9159; found, 525.9155.

2.4 Synthesis of 4-[N,N-di(4- phenyl-9H-carbazol)amino]benzaldehyde (3)

Firstly, 1.05 g of **2** (2 mmol), 1.43 g of **1** (5 mmol) and 0.18 g (0.03 mmol) of $Pd[P(Ph)_3]_4$ were mixed into a 100 mL flask. Then, 5 mL of 2 M K_2CO_3 solution and 30 mL of THF were added and refluxed for 24 h under nitrogen atmosphere. After reaction, 100 mL of distilled water was introduced and stirred vigorously, then the organic layer was extracted by 50 mL of DCM. The obtained DCM layer was washed repeatedly by saturated brine and dried with 10 g of $MgSO_4$. The dried organic layer was concentrated under reduced pressure and purified by silica-gel column chromatography using CH_2Cl_2/petroleum ether (volume ratio gradually changed from 2:1~1:1) as eluent. Finally, the yellow-green pure product was collected with a yield of 63.2%. ^{1}H NMR (400 MHz, $CDCl_3$), δ (TMS, ppm): 9.70 (s, 1H), 7.45 (d, J = 6.6 Hz, 4H), 7.35 (m, J = 7.6 Hz, 12H), 7.26 (d, J = 6.4 Hz, 8H), 7.22 (m, J = 9.6 Hz, 8H), 7.03 (d, J = 7.8 Hz, 2H), 6.97 (d, J = 5.6 Hz, 2H). ^{13}C NMR (100 MHz, $CDCl_3$), δ (TMS, ppm):115.67, 121.85, 122.88, 123.92, 124.42, 126.47, 127.09, 130.30, 130.68, 131.22, 135.38, 136.21, 146.72, 192.95. HRMS (m/z): $[M+H]^+$ calcd. for $C_{55}H_{37}N_3O$, 756.3009; found, 756.2999.

2.5 Synthesis of TPA-DCV

0.85 g of **3** (1 mmol) and 0.13 g of malonitrile (2 mmol) were added into 30 mL of CH_2Cl_2 solution. This reaction could be completed by stirring 6 h at 25 °C. The mixtures were concentrated directly and further purified by silica gel column chromatography to afford a pure product with 58.3% yield. ^{1}H NMR (400 MHz, $CDCl_3$), δ (TMS, ppm): 8.01 (s, 1H), 7.49 (d, J = 7.8 Hz, 4H), 7.32 (m, 16H), 7.20 (m, J = 7.2 Hz, 6H), 7.04 (t, J = 8.2 Hz,6H), 6.87 (d, J = 7.8 Hz,2H), 6.83 (d, J = 8.4 Hz,2H). ^{13}C NMR (100 MHz, $CDCl_3$), δ (TMS, ppm): 158.96, 141.39, 133.38, 132.82, 131.22, 130.94, 128.26, 125.93, 125.34, 123.34, 120.35, 119.94, 113.82, 109.79, 82.39. HRMS (m/z): $[M+H]^+$ calcd. for $C_{58}H_{37}N_5$, 804.3127; found, 804.3121.

2.6 Experimental details for anion sensing

The detection system was obtained by rapidly injecting the DMSO solution of TPA-DCV (50

μL, 2.0 mM) into the micellar solution of CTAB (5 mL, 2.0 mM) in water under rigorous stirring for 60 seconds. For the CN^- detection, 2 mL of sensor solution (TPA-DCV, 20 μM; CTAB, 2.0 mM) was first added into quartz cuvette, then different concentrations of CN^- were added sequentially. The spectra signals were recorded after 2 min using absorption and fluorescence spectra. The response of sensor to other anions were carried out using the uniform procedure to that of CN^-.

2.7 Detection of trace water and CN^- using smartphone and LDA integrated detection system.

The detection system mainly relied on smartphone and LDA. Smartphone was used to take photos of the fluorescence and extracted the red, green and blue parameters of the fluorescence color. LDA was used to intelligently identify and classify the color, and established the relationship between color distribution and the concentration of substances. The fluorescence photo of samples must be taken in completely dark environment under a 365 nm UV lamp, and the phone should be fixed at 20 cm in front of the sample. The obtained fluorescence photos were scanned using the smartphone APP (Color Recognizer) for color component analysis to extract red, green and blue channel parameters. To ensure the accuracy and comprehensiveness of extraction, 6 different locations in the photo were randomly selected for color parameter extraction. These extracted parameters were then injected into the LDA for further separation and classification.

For the detection of trace water in different organic solvents, 20 μM of TPA-DCV solution in different pure organic solvents were first prepared, then different water content was introduced in turn. After each addition, the fluorescent color of the solution was recorded by smartphone and analyzed by LDA. For the detection of CN^-, a simple and portable test strip was first prepared by immersing cellulose filter papers in the stock solutions of TPA-DCV (1 mM) for 5 minutes, and then drying it by exposure to air. The prepared test strips were immersed in different concentrations of standard CN^- solution, and took corresponding fluorescent photos. The following color parameter extraction and unknown samples analysis were carried out according to the steps mentioned above.

2 Results and discussion

3.1 Synthesis and characterization of TPA-DCV

TPA-DCV was synthesized in a moderate yield according to the procedures displayed in **Scheme 1**. Briefly, 3-bromo-*N*-phenylcarbazole was first added into a lithiated THF solution of trimethyl borate and then hydrolyzed in hydrochloric acid to form 9-phenyl-9*H*-carbazole-3-boronic acid (1). 4-di(4-iodophenyl)aminobenzaldehyde (2) could be obtained in the presence of potassium iodate and potassium iodide, which reacted with **1** to give a yellow solid 4-[N,N-di(4-phenyl-9H-carbazol)amino]benzaldehyde (**3**) [32]. After subsequent Knoevenagel reaction with excess malononitrile in dichloromethane, the target product was obtained. The synthetic products were all characterized by HRMS ^{1}H NMR and ^{13}C NMR, and satisfactory data that consistent with its structure were obtained (**Fig. S13-Fig. S23**).

3.2 Solvatochromism of TPA-DCV

The presence of electron donor TPA framework and electron acceptor DCV signify that TPA-DCV has typical donor (D)-π-acceptor (A) structure. Molecules with a D-A structure are well known for their significant solvatochromic effect, and their optical properties are highly rest upon solvent polarity. Hence, the spectral properties of TPA-DCV in different solvents were carefully investigated and the results were depicted in **Fig. 1**. With solvent polarity increasing from weak polar toluene to strong polar DMF, the emission peaks of TPA-DCV were gradually red-shifted from 474 nm to 603 nm, displaying an obvious fluorescence color transform from blue to red which nearly covered the full visible spectrum. Meanwhile, the red shift of the emission was accompanied by a significant decrease in intensity **(Fig. S1)**. On the contrary, the absorption of TPA-DCV exhibited minor changes on changing the solvent polarity **(Fig. S2)**. These phenomena showed that the optical properties of TPA-DCV were controlled by solvent polarity, which was caused by the ICT effect from electron donor TPA framework to electron acceptor DCV.

3.3 Aggregation induced emission effect (AIE)

Besides solvatochromism effect, TPA-DCV also exhibits a typical AIE feature. As displayed in **Fig. S4**, the pure MeCN solution of TPA-DCV was almost nonemissive. However, the fluorescence intensities abruptly enhanced when water content increased to 30%, and then gradually decreased when content exceeded 70%. A more interesting phenomenon can be observed when replacing MeCN with DMF. As depicted in **Fig. 2**, the red emission of TPA-DCV showed sustained decrease until the water content reached to

30%. Meanwhile, a slight red shift of emission peak was observed. This phenomenon could be reasonably explained by the enhancement of ICT effect. Upon further increasing water content from 30% to 60%, a dramatic enhance in fluorescence intensity (400-fold) along with a large-scope blue shift in PL peak from 603 nm to 512 nm were observed. The increase in water content led to the aggregation of TPA-DCV, thereby restraining the rotation of the TPA-DCV molecules and resulting in a strong emission of the aggregates. Meanwhile, aggregation made the molecules be confined in a non-polar environment, which could partially impede the ICT process and was also helpful for the emission enhancement [33-35]. Abnormally, when water content increased from 70% to 90%, the fluorescence intensity significant decrease and slightly red-shifted again. This phenomenon may be induced by the crystallization-induced emission effect of TPA-DCV. The TPA-DCV tend to form crystalline aggregates at low levels of water while less emissive, redder amorphous aggregates with smaller size will be formed at high water fractions[36].

3.4 Intelligent and rapid determination of trace water

The emission of TPA-DCV in different solvents by adding different amounts of water were carefully investigated. As shown in **Fig. 3a**, the emission intensity decreased drastically when water content was below 1% and the relative fluorescence decreased by 88%, 62%, 55% and 50% in ethyl acetate (EA), benzene (Ben), THF and dichloromethane (DCM), respectively. Moreover, the emission peak showed a good linear relationship with the water content in low water region. The detection limits of TPA-DCV for water were 79 ppm, 73 ppm, 130 ppm and 54 ppm in Ben, EA, THF and DCM, respectively (**Fig. S5-S8**).

However, this traditional fluorescence detection mode is still not convenient enough. We here introduce LDA and smartphone integrated detection system for intelligent and rapid water measurement without any instrument testing. As shown in **Fig. 3b**, through the extraction of red, green and blue channels of fluorescent colors by smartphone, combined with LDA, the fluorescence colors that were difficult to distinguish could be clearly and correctly classified. What's more, different water contents in different solvents were found to be linearly distributed in the LDA canonical score plot. This means that the category of organic solvent and the water content of the solvent can be analyzed only by analyzing the fluorescence color of the sample. To verify our conjecture, we randomly added different amounts of water to different solvents and labeled sample 1, 2, 3 and 4. Then we reduced the amount of water added by half and marked it as sample 5, 6, 7 and 8. The fluorescence colors of samples was recorded by smartphone and then

accurately classified by LDA. As shown in **Fig. 3b**, the results suggested that sample 1 was benzene solvent with an approximate 0.6% water content. The solvent of sample 5 was also classified as benzene, and the water content was shown to be between 0.3% and 0.4%, which was basically consistent with the addition amount. The rest of the samples were distributed on their respective curves, which not only clarified their categories but also their water content. The accurate solvent classification and water content detection preliminarily demonstrate the reliability of the proposed detection system.

3.5 Fluorescence detection of CN^- in aqueous solution

The fluorescence detection of CN^- is mainly realized by the reaction between strong nucleophilicity of the CN^- and probe. However, the efficiency of nucleophilic addition is significantly reduced by water, making the reaction-based CN^- probe difficult to work efficiently in water.[37, 38]. Considering the typical AIE characteristics of the TPA-DCV, we envision that the TPA-DCV may be utilized as a fluorescent detector for sensing of CN^- based on the AIE effect. The envisaged detection mechanism is described briefly in **Scheme 2**. TPA-DCV should be able to stably disperse in aqueous media and exhibit strong greenish yellow fluorescence with the help of CTAB (**Fig. S9**).[33, 39] After adding the CN^-, the aggregates would be disassembled and the strong emission induced by AIE feature would be selectively quenched or weaken owing to the formation of negatively charged water-soluble products. In addition, the nucleophilic addition would destroy the conjugate structure between TPA skeleton and reactive unit and further caused significant changes in absorption.

Indeed, the nucleophilic addition reaction between CN^- and TPA-DCV can destroy the aggregates and quench the emission in aqueous solution. As shown in **Fig. 4a**, the increase of CN^- resulted in an obvious fluorescence decrease at 528 nm and was accompanied by a significant blue shift from 528 nm to 489 nm. This blue shift was attributed to the destruction of extensive π-conjugation of TPA-DCV after the nucleophilic addition of CN^- and DCV. The destruction of conjugate construction also caused dramatic changes in the absorption signal. As depicted in **Fig. 4b**, the strong absorption bands at 329 nm and 403 nm that was assigned to the $\pi \rightarrow \pi^*$ transition of the conjugated system was gradually weaken as the CN^- concentration increases until they disappear. Accordingly, the color

transformed from faint yellow to colorless. Meanwhile, a new band appeared at 281 nm and enhanced with increasing CN^- concentration.

Further evidences for the nucleophilic addition of TPA-DCV with CN^- were obtained from the ^1H NMR titration experiments in $CDCl_3$. As shown in **Fig. 5**, the protons of olefinic at 8.01 ppm disappeared completely after reaction with CN^-, while a new proton peak appeared at 4.41 ppm. This result confirmed that the CN^- attacked the DCV and turned C=C into C-C [40]. It is noteworthy that the signal of the β-proton in the malononitrile moiety was missing after the reaction with CN^-, implying the TPA-DCV formed a stable anionic species TPA-DCV-CN^- [38]. Such a stable water-soluble species supported the proposed quenching mechanism that the aggregated TPA-DCV were disaggregated after the addition of CN^- and thus quenched the AIE induced emission. In addition, more intuitive evidence for the nucleophilic addition of TPA-DCV with CN^-can be obtained from HRMS results. As shown in Fig. S10, the found value 830.3154 was consistent with the calculated value 830.3148, which further confirmed the accuracy of the proposed mechanism.

We also noted that the fluorescence decrease was saturated when 5.5 equiv. of CN^- was added, which was less than the amount required for most of the reported reaction-based CN^- sensors (**Table S1**) In the range of 0 to 5 μM, an excellent linear relationship could be obtained with a correlation coefficient of 0.99157 (**Fig. S11**). The detection limit was calculated to be 0.16 μM, which was lower than the guideline of CN^- permitted by the EPA (1.9 μM) **(Table S2)**. The extreme sensitivity of TPA-DCV to CN^- was attributed to the introduction of CTAB, which provided a hydrophobic space that greatly reduces the interference of water on nucleophilic reactions.

Although TPA-DCV exhibits significant spectral changes to CN^-, the interference of other anions such as fluoride and acetate cannot be neglected. We herein carefully investigated the selectivity of TPA-DCV for different anions ($H_2PO_4^-$, AcO^-, ClO_4^-, HSO_3^-, CN^-, F^-, Cl^-, Br^- and I^-) by using fluorescence and UV-vis spectroscopy. As displayed in **Fig. 6**, the fluorescence of TPA-DCV was significantly quenched and the color transformed from green to light blue when 5 equiv. of CN^- was added. Similarly, the absorption spectrum also exhibited significant changes, and the color changed from yellow to colorless. However, the addition of higher concentrations of other ions almost had no effect on the spectral signal, as well as the color. This result demonstrated the excellent selectively of TPA-DCV toward CN^-. The interference experiments further confirmed

that the selective detection of CN^- was almost unaffected by the coexisting ions even if the interference ions concentration was much higher (**Fig. S12**). In addition, the analysis of natural water samples and standard addition recovery experiments were also carried out to investigate the reliability and practicality of the TPA-DCV CTAB probe. As shown in **Table S3,** the recovery of CN^- were statistically close to 100%, confirming the good reliability of the proposed method.

3.6 Intelligent and rapid detection of CN^-

Effective determination of CN^- in water solution is an encouraging progression. But it is still not convenient enough for rapid on-site detection, which remains a challenge. For this purpose, we first developed a cellulose paper-based test strip. As shown in **Fig. 7a**, the test strips displayed bright green fluorescence in the absence of CN^-. As the concentration of CN^- increased from 0 to 20 ppm, the fluorescent colors of the test paper were significantly darkened. This phenomenon confirmed that the test strips was highly desirable for rapid and intuitive detection of CN^-. However, to construct proportional relationship between fluorescence color and CN^- concentration just by naked eyes was not advisable and accurate. To clarify the exact relationship between fluorescence color and CN^- concentration, a smartphone and LDA integrated detection system had been developed. As shown in **Fig. 7b**, through the extraction of red, green and blue parameters of test strips fluorescent colors by smartphone, combined with LDA, the colors that were difficult to distinguish could be clearly and correctly classified in 3D and 2D (**Fig. 7c**) canonical score plot. Different concentrations were arranged in space with a specific curve, which made quantitative analysis of CN^- become possible.

A large number of real water samples that spiked with different concentrations of CN^- were tested to verify the practicability. The test strip was first immersed in the real water sample for 3 minutes, then the fluorescent photo was taken and extracted by the smartphone, and finally the color parameter was injected into the LDA for intelligent classification. As shown in **Fig. 7d**, the classifications of the blank samples of the three real water samples were identical to the classifications of the standard blank samples. When the CN^- concentration was increased to 2, 6, 10 and 20 ppm, the corresponding classifications of real water samples were partially slightly deviated from the standard sample, and the suggested concentrations were basically consistent with the spiked values. The three real samples also did not show significant differences in the classification. These results demonstrated the satisfactory stability and accuracy of the proposed detection system. More importantly, with the integration of visual test strip assisted by smartphone and LDA, the quantitative analysis of CN^- in the real water samples was greatly simplified,

eliminating the requirement for instrument testing, realizing rapid, portable, on-site inspection.

Conclusion

In summary, a new intelligent and rapid detection system based on an AIE fluorophore TPA-DCV was established for portable and on-site detection of trace water in organic solvents and CN^- in water. The TPA-DCV not only displays remarkable solvatochromism effect and shows different fluorescence colors to different water contents of different solvents, but also exhibits specific response to CN^- and shows significant fluorescence changes. These different fluorescent color signals can be accurately classified in canonical score plot after being captured and extracted by smartphone and separated by LDA. What's more, the color distribution in the space and the concentration of the detection target show regular changes, which makes quantitative analysis possible. The rationality and practicability of this detection system are preliminary verified by a large number of actual sample analyses. Of course, it could be argued that this detection is not precise, indeed, but we think significance of this detection system is in the proof of intelligent and rapid detection of multiple targets just using a simple color analysis without any instrument test, which may be a big step forward. We also believe that this kind of convenient and portable detection method will be further developed by using more advanced algorithms or artificial intelligence network, which is also the direction of our efforts.

Acknowledgments

We are grateful to the Natural Science Foundation of China (No. 41807200, 41773126, 51878633) for their financial assistance. We also sincerely thank the Foundation for Innovative Research Groups of the National Natural Science Foundation of China (No. 41521001) and the "Fundamental Research Funds for the Central Universities" for financial support.

References

[1] Peng MJ, Guo Y, Yang XF, Wang LY, An J. A highly selective ratiometric and colorimetric chemosensor forcyanide detection. Dyes Pigments 2013;98(3):327-2.

[2] Ma J, Dasgupta PK. Recent developments in cyanide detection: a review. Anal Chim Acta 2010;673:117-125.

[3] Badugu R, Lakowicz JR, Geddes CD. Enhanced fluorescence cyanide detection at physiologically lethal levels: reduced ICT-based signal transduction. J Am Chem Soc 2005;127:3635-41.

[4] Shan D, Christine Mousty A, Cosnier S. Subnanomolar Cyanide Detection at Polyphenol Oxidase/Clay Biosensors. Anal Chem 2004;76:178-83.

[5] Kemmei T, Kodama S, Yamamoto A, Inoue Y, Hayakawa K. Determination of Low-Level Ethylenediaminetetraacetic Acid in Water Samples by Ion Chromatography with Ultraviolet Detection. Chromatographia 2007;65:229-32.

[6] Shen P, Li M, Liu C, Yang W, Liu S, Yang C. Two Sensitive Fluorescent BOPIM Probes with Tunable TICT Character for Low-Level Water Detection in Organic Solvents. J Fluoresc 2016;26:363.

[7] Hisamoto H, Manabe Y, Yanai H, Tohma H, Yamada T, Suzuki K. Molecular Design, Characterization, and Application of Multiinformation Dyes for Multidimensional Optical Chemical Sensings. Anal Chem 1998;70:1255.

[8] Citterio D, Minamihashi TK, Kuniyoshi Y, Hisamoto H, Sasaki S, Suzuki K. Optical determination of low-level water concentrations in organic solvents using fluorescent acridinyl dyes and dye-immobilized polymer membranes. Anal Chem 2001;73:5339-45.

[9] Ding L, Zhang Z, Li X, Su J. Highly sensitive determination of low-level water content in organic solvents using novel solvatochromic dyes based on thioxanthone. Chem Commun 2013;49:7319-21.

[10] Nie HM, Gong CB, Qian T, Ma XB, Chow CF. Visual and reversible detection of cyanide ions in protic solvents by a novel colorimetric receptor. Dyes Pigments 2014;106:74-80.

[11] Isaad J, Achari AE, Malek F. Bio-polymer starch thin film sensors for low concentration detection of cyanide anions in water. Dyes Pigments 2013;97:134-40.

[12] Chen X, Nam SW, Kim GH, Song N, Jeong Y, Shin I, et al. A near-infrared fluorescent sensor for detection of cyanide in aqueous solution and its application for bioimaging. Chem Commun 2010;46:8953-5.

[13] Shan D, Cosnier S, Mousty C. HRP/[Zn–Cr–ABTS] redox clay-based biosensor: design and optimization for cyanide detection. Biosens Bioelectron 2005;20:390-6.

[14] Chen L, Tian X, Zhao Y, Li Y, Yang C, Zhou Z, Liu X, A ratiometric fluorescence nanosensor for highly selective and sensitive detection of selenite, Analyst 2016;141:4685-93.

[15] Tian X, Hui P, Yong L, Chao Y, Zhou Z, Wang Y. Highly sensitive and selective paper sensor based on carbon quantum dots for visual detection of TNT residues in groundwater. Sens Actuators B 2017;243:1002-9.

[16] Chen L, Tian X, Yang C, Li Y, Zhou Z, Wang Y, et al. Highly selective and sensitive determination of copper ion based on a visual fluorescence method. Sens Actuators B 2017;240:66-75.

[17] Jarangdet T, Pratumyot K, Srikittiwanna K, Dungchai W, Mingvanish W, Techakriengkrai I, et al. A fluorometric paper-based sensor array for the discrimination of volatile organic compounds (VOCs) with novel salicylidene derivatives. Dyes Pigments 2018;159:378-83.

[18] Juanjuan LU, Shenguang GE, Lei GE, Mei Y, Jinghua YU. Electrochemical DNA sensor based on three-dimensional folding paper device for specific and sensitive point-of-care testing. Electrochim Acta 2012;80:334-41.

[19] Wang HH, Xue L, Yu CL, Qian YY, Jiang H. Rhodamine-based fluorescent sensor for mercury in buffer solution and living cells. Dyes Pigments 2011;91:350-5.

[20] Hossain SMZ, Brennan JD, Chem A. β-Galactosidase-based colorimetric paper sensor for determination of heavy metals. Anal Chem 2011;83:8772-8.

[21] Tian X, Chen L, Li Y, Yang C, Nie Y, Zhou C. Design and synthesis of a molecule with aggregation-induced emission effects and its application in the detection of arsenite in groundwater. J Mater Chem C 2017;5:3669-72.

[22] Zhang H. Quaternion Zernike moments and their invariants for color image analysis and object recognition. Signal Process 2012;92:308-18.

[23] Shenghong Y. Wenjing G. Xiaohan S. Electrostatic association complex of a polymer capped CdTe(S) quantum dot and a small molecule dye as a robust ratiometric fluorescence probe of copper ions. Dyes Pigments 2018;158:114-120.

[24] He W, Luo L, Liu Q, Chen Z. Colorimetric Sensor Array for Discrimination of Heavy Metal Ions in Aqueous Solution Based on Three Kinds of Thiols as Receptors. Anal Chem 2018;90:4770-75.

[25] Jing W, Lu Y, Yang G, Wang F, He L, Liu Y. Fluorescence sensor array based on amino acids-modulating quantum dots for the discrimination of metal ions. Anal Chim Acta 2017;985:175.

[26] Tan L, Chen Z, Zhao Y, Wei X, Li Y, Zhang C, et al. Dual channel sensor for detection and discrimination of heavy metal ions based on colorimetric and fluorescence response of the AuNPs-DNA conjugates. Biosens Bioelectron 2016;85:414-21.

[27] Mao J, Lu Y, Chang N, Yang J, Zhang S, Liu Y. Multidimensional colorimetric sensor array for discrimination of proteins. Biosens Bioelectron 2016;86:56-61.

[28] Xu W, Ren C, Teoh CL, Peng J, Gadre SH, Rhee HW, et al. An artificial tongue fluorescent sensor array for identification and quantitation of various heavy metal ions. Anal Chem 2014;86:8763-9.

[29] Kang Q, Peng L. An extended PCA and LDA for color face recognition. International Conference on Information Security and Intelligence Control. IEEE 2012;348-48. https://ieeexplore.ieee.org/document/6449777

[30] Zhou R, Li F, Wang Y, Zheng XY, Zhao RW, Li GZ. Application of PCA and LDA methods on gloss recognition research in TCM complexion inspection. International Conference on Bioinformatics and Biomedicine Workshops. IEEE 2010;666-69. https://ieeexplore.ieee.org/document/5703884

[31] Thomas M, Kambhamettu C, Kumar S. Face Recognition Using a Color Subspace LDA Approach. 20th International Conference on Tools with Artificial Intelligence. IEEE 2008;231-235. https://ieeexplore.ieee.org/document/4669694

[32] Wang B, Wang Y, Hua J, Jiang Y, Huang J, Qian S, et al. Starburst triarylamine donor-acceptor-donor quadrupolar derivatives based on cyano-substituted diphenylaminestyrylbenzene: tunable aggregation induced emission colors and large two-photon absorption cross sections. Chemistry 2011;17:2647-55.

[33] Zhang Y, Li D, Li Y, Yu J. Solvatochromic AIE luminogens as supersensitive water detectors in organic solvents and highly efficient cyanide chemosensors in water. Chem Sci 2014;5:2710-6.

[34] Kang M, Gu X, Kwok RT, Leung CW, Lam JW, Li F, et al. A near-infrared AIEgen for specific imaging of lipid droplets. Chem Commun 2016;52:5957-60.

[35] Li H, Wang Z, Li J, Zhao E, Sun JZ, Lam JWY, et al. Facile Preparation of Light Refractive Poly(aroxycarbonyltriazole)s by Metal-Free Click Polymerization. Macromol Chem Phys 2014;215:1036–41.

[36] Dong Y, Lam JW, Qin A, Sun J, Liu J, Li Z, et al. Aggregation-induced and crystallization-enhanced emissions of 1,2-diphenyl-3,4-bis(diphenylmethylene)-1-cyclobutene. Chem Commun 2007;43:3255.

[37] Vallejos S, Kaoutit HE, Estévez P, García FC, Serna F, et al. Working with water insoluble organic molecules in aqueous media: fluorene derivative-containing polymers as sensory materials for the colorimetric sensing of cyanide in water. Poly Chem 2011;2:1129-38.

[38] Lee CH, Yoon HJ, Shim JS, Jang WD. A BoradiazaindacenE-Based TurN-On Fluorescent Probe for Cyanide Detection in Aqueous Media. Chem-Eur J 2012;18:4513.

[39] Hu R, Feng J, Hu D, Wang S, Li S, Li Y, et al. A Rapid Aqueous Fluoride Ion Sensor with Dual Output Modes. Angew Chem Int Edit 2010;49:4915-8.

[40] Hong SJ, Yoo J, Kim SH, Kim JS, Yoon J, Lee CH. ChemInform Abstract: β-Vinyl Substituted Calix[4]pyrrole as a Selective Ratiometric Sensor for Cyanide Anion. Cheminform 2009;40:189-91.

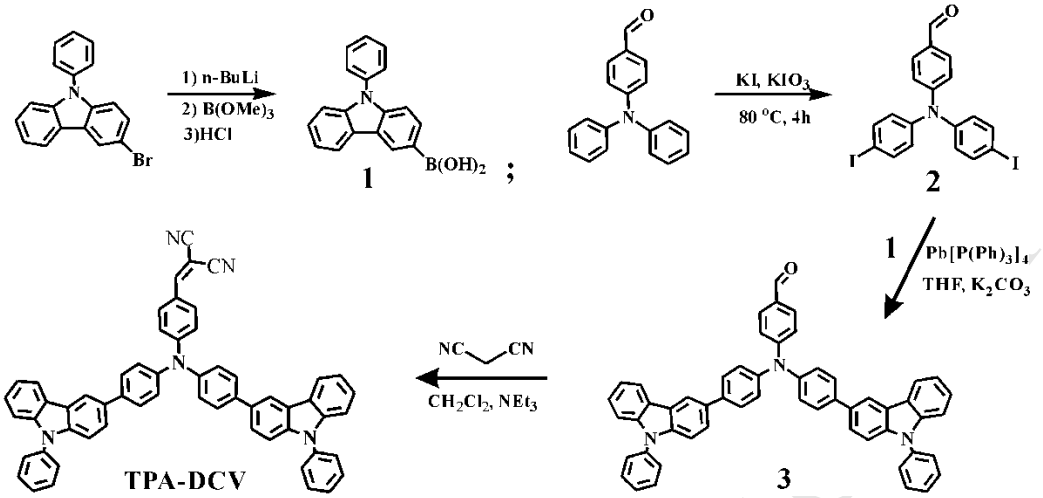

Scheme 1 Synthetic route for TPA-DCV

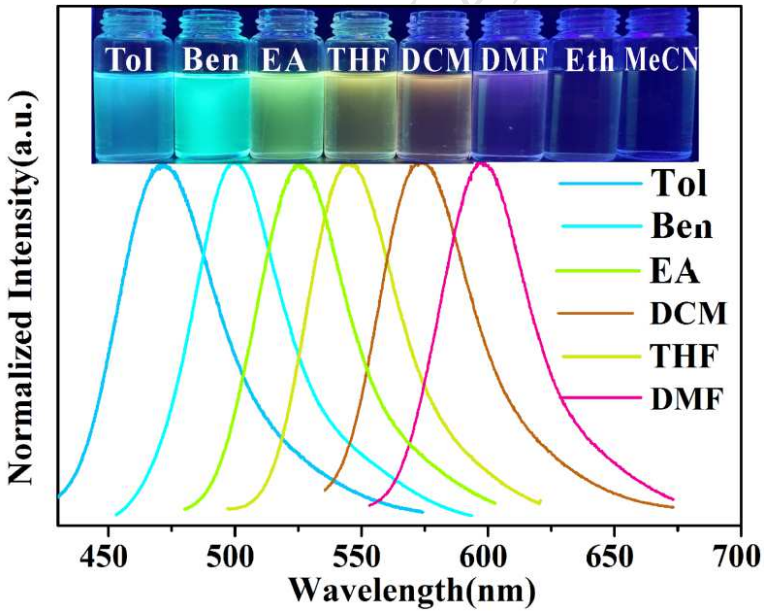

Fig. 1. (a) Normalized fluorescence spectra of TPA-DCV (20 μM) in different pure solvents. Photographs of TPA-DCV in different solvents were taken under 365 nm UV lamp (Tol, toluene; Ben, benzene, EA, ethyl acetate; DCM, dichloromethane; MeCN, acetonitrile). Excitation wavelength: 390 nm.

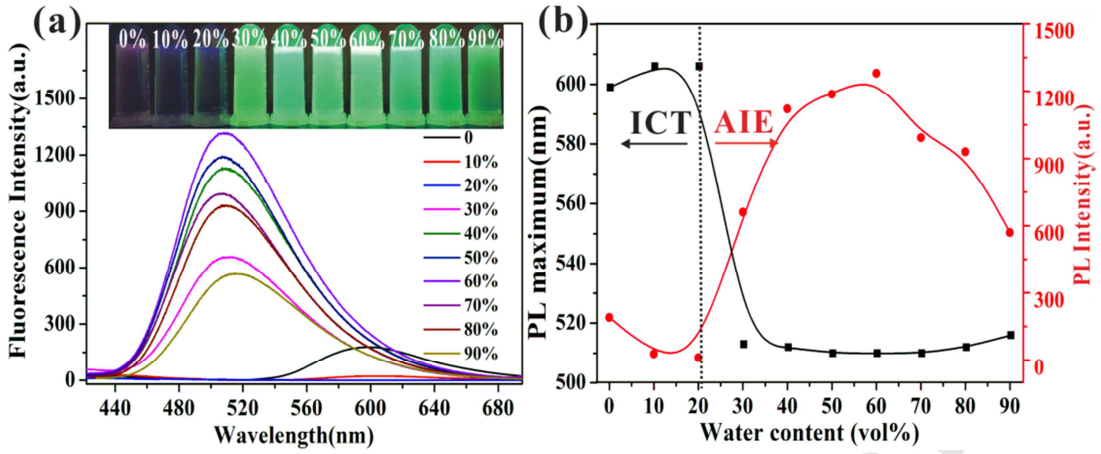

Fig. 2. (a) Fluorescence spectra of TPA-DCV in DMF-water mixtures with different water content. Inset: the corresponding fluorescence images of TPA-DCV solutions under 365 nm UV lamp. (b) Plots of fluorescence maximum and fluorescence intensity *vs.* the water content of the DMF-water mixtures. Excitation wavelength: 390 nm.

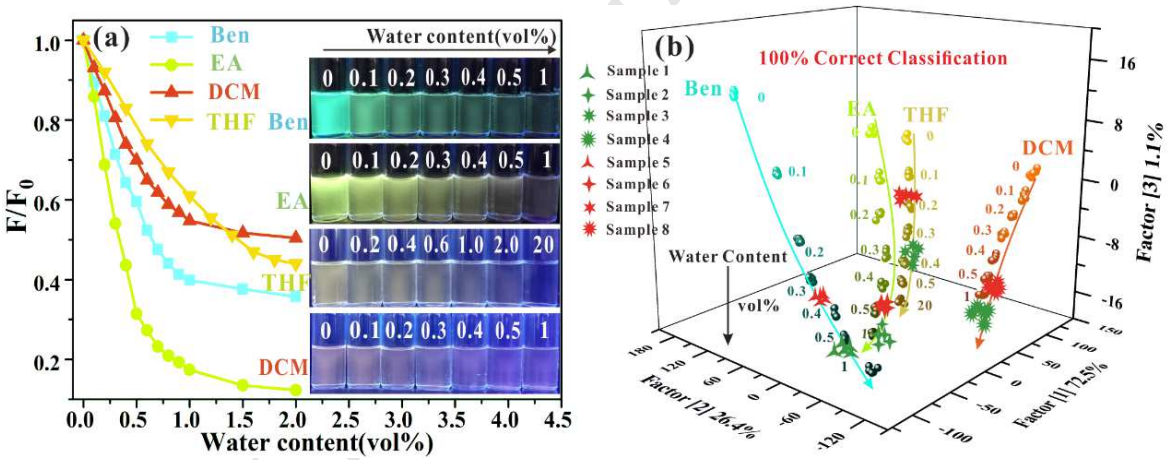

Fig. 3. (a) Plot of F/F_0 *vs.* different water content in different solvents (F: the fluorescence maximum; F_0: the fluorescence maximum in pure solvent). Inset: the fluorescence photographs of TPA-DCV solution with different water content. (b) 3D LDA canonical score plot of TPA-DCV fluorescence color response to different water content of different organic solvents. Samples 1-8 are randomly prepared samples (five trials each).

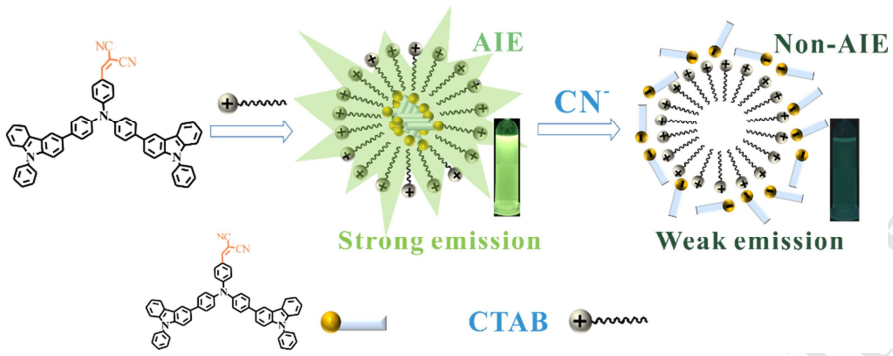

Scheme 2. Schematic illustration of the TPA-DCV formation of aggregates in CTAB solution and the disintegration of the aggregates in the presence of CN^-

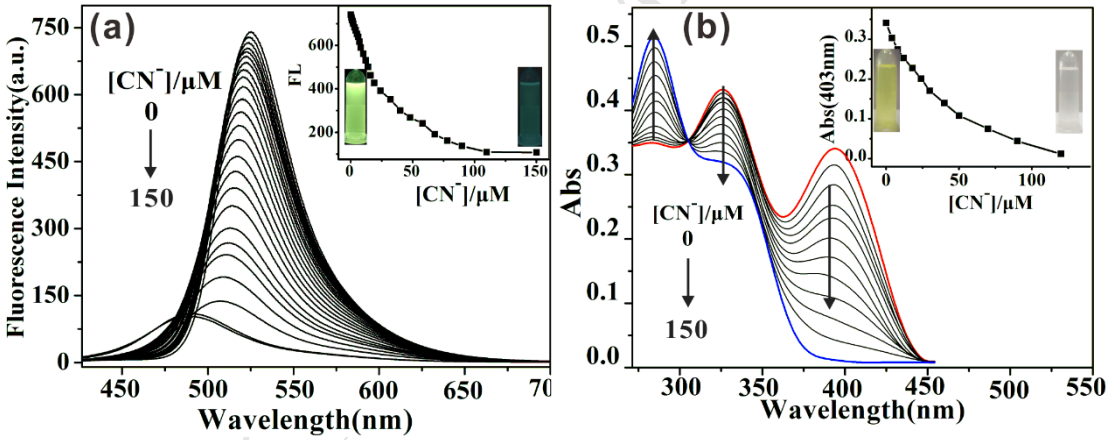

Fig. 4. (a) Fluorescence (b) emission spectra changes of TPA-DCV (20 μM) upon the addition of 0-5.5 equiv. of CN^- in 2 mM CTAB micellar. Inset: plot of (a) fluorescence maximum (b) absorption intensity (403 nm) *vs.* different CN^- concentration. Images: the left is none of CN^- and right is 5.5 equiv. of CN^-.

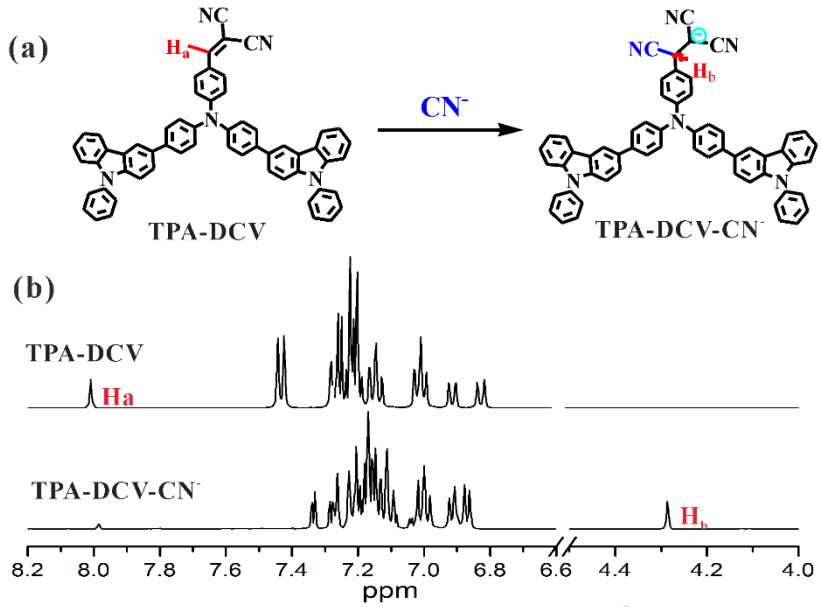

Fig. 5. (a) Reaction mechanism between TPA-DCV and CN^-. (b) ^1H NMR spectra of TPA-DCV before and after the addition of CN^- in $CDCl_3$.

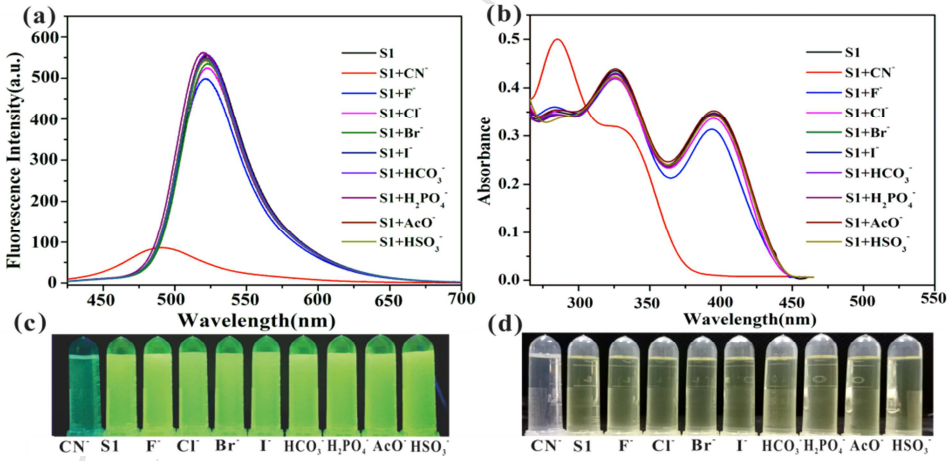

Fig. 6. (a)Fluorescence and (b) absorption spectra of TPA-DCV (20 μM) in CTAB micelles (2 mM) upon addition of different anions (CN^-: 5 equiv., other anions: 25 equiv.). The corresponding (c) emission and (d) color changes of TPA-DCV in CTAB micelles solution (2 mM) upon addition of various anions. Excitation wavelength: 390 nm.

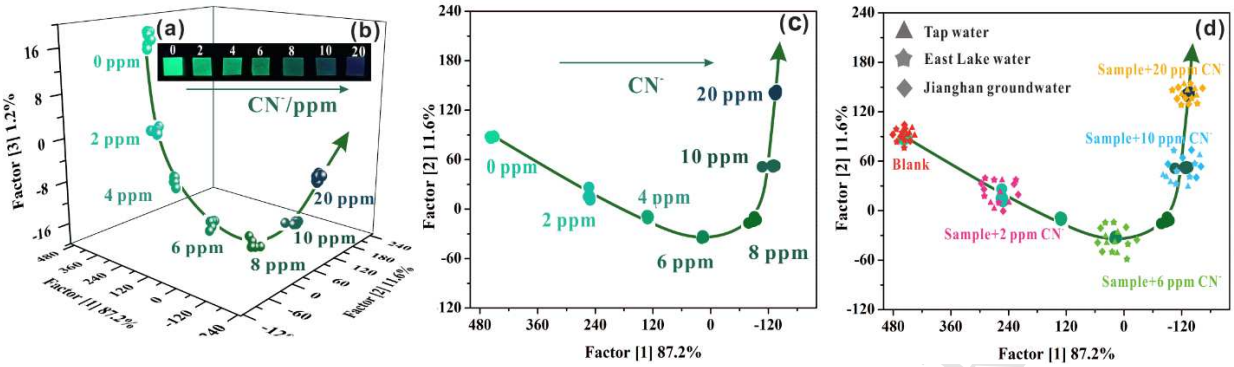

Fig. 7. (a) The photos of the test strip under UV light (365 nm) after exposure to different concentrations of CN^-. (b) 3D LDA canonical score plot shows for the response of test trips to different concentrations of CN^-. (c) Corresponding 2D LDA canonical score plot for the response of test trips to different concentrations of CN^-. (d) 2D LDA canonical score plot for the real water samples test (five trials each).

Highlights

1. An AIE dye TPA-DCV that exhibits both AIE and solvatochromic effects has been developed for effective recognition of trace water and CN^-.

2. An AIE dye based smartphone and LDA integrated portable, intelligent and rapid detection system for trace water and CN^- is first time established.

3. The water content and CN^-concentration can be rapid and intelligent detected using the integrated system without any instrument testing.